Supporting Information

Surface acidity modulates the peroxidase-like activity of nanoclay

Hao Wang[abc], Muhammad Tariq Sarwar[abc], Wenxin Bao[abc], Luyuan Tian[abc], Huaming Yang[abcd *]

[a] *Engineering Research Center of Nano-Geomaterials of Ministry of Education, China University of Geosciences, Wuhan 430074, China*

[b] *Faculty of Materials Science and Chemistry, China University of Geosciences, Wuhan 430074, China*

[c] *Key Laboratory of Functional Geomaterials in China Nonmetallic Minerals Industry, China University of Geosciences, Wuhan 430074, China*

[d] *Hunan Key Laboratory of Mineral Materials and Application, School of Minerals Processing and Bioengineering, Central South University, Changsha 410083, China*

[*]Corresponding author

Email: hm.yang@cug.edu.cn, hmyang@csu.edu.cn (H. Yang).

Experimental Section

Materials and reagents

$LiNO_3$, $NaNO_3$, KNO_3, NaOH, iron chloride hexahydrate ($FeCl_3 \cdot 6H_2O$), ammonium chloride (NH_4Cl), ammonia solution ($NH_3 \cdot H_2O$), hydrogen peroxide (H_2O_2) were acquired from Sinopharm Chemical Reagent Co., Ltd. (China). Iron nitrate nonahydrate ($Fe(NO_3)_3 \cdot 9H_2O$), iron (II) chloride tetrahydrate ($FeCl_2 \cdot 4H_2O$), terephthalic acid (TA), and o-phenylenediamine (OPD) were obtained from Aladdin Chemistry Co., Ltd. (China). 3,3',5,5'-tetramethylbenzidine (TMB), iron sulfate hydrate ($Fe_2S_3O_{12} \cdot xH_2O$), and 2,2'-azinobis(3-ethylbenzothiazoline-6-sulfonic acid ammonium salt) (ABTS) were purchased from Macklin Biochemical Technology Co., Ltd. (China). Montmorillonite (MMT, CAS NO. 1318-93-0) was obtained from Cheng Du Micxy Chemical Co., Ltd. (China). All reagents were used directly without purification. All aqueous solutions were made using ultrapure water (18.25 MΩ·cm).

Instrumentations

Scanning electron microscopy (SEM) and transmission electron microscopy (TEM) were taken using a ZEISS GeminiSEM 300 (Germany) and a JEOL JEM 2100F (Japan), respectively. Atomic force microscopy (AFM) was recorded via a Dimension Icon (Bruker, Germany). Temperature programmed desorption of ammonia (NH_3-TPD) and temperature programmed reduction of hydrogen (H_2-TPR) were analyzed by Bel Cata II (USA). X-ray powder diffraction (XRD) patterns were performed on a D8 ADVANCE (Bruker, Germany). An inductively coupled plasma optical emission spectrometer (ICP-OES) was taken using an ARL PERFORM'X (Thermo, USA). X-ray photoelectron spectroscopy (XPS) was recorded

using an ESCALAB 250Xi (Thermo Scientific, USA). The X-ray absorption spectra (XAS) of the samples at Fe K-edge were recorded at the Beamline of TPS44A1 at the National Synchrotron Radiation Research Center (NSRRC), Taiwan. The absorbance of the colorimetric reaction product was recorded by a microplate reader (SPARK, Tecan, Austria).

Synthesis of MMT-Na

MMT and alkali nitrate ($LiNO_3$, $NaNO_3$, or KNO_3) were mixed thoroughly in a mortar, and then the mixture was transferred to an alumina boat. Subsequently, it was placed in a muffle furnace and heated to 350 ℃ for 4 h (10°/min). After cooling to room temperature, the solids were washed several times with deionized water. Exfoliated MMT was obtained after freeze-drying. The corresponding products of alkali nitrate $LiNO_3$, $NaNO_3$, and KNO_3 are named MMT-Li, MMT-Na, and MMT-K, respectively. Hectorite was used to replace MMT, $NaNO_3$ was selected as molten salt, and the product obtained under the same reaction conditions was named Hectorite-Na.

Synthesis of Fe/MMT-Na

MMT-Na was mixed with 150 mL of deionized water and exposed to ultrasound for 1 hour. The mixed solution was heated to 85 ℃, then $Fe_2S_3O_{12}{\cdot}xH_2O$ was added under stirring. After another 1 h, the solution was centrifuged, and the solid was washed several times with deionized water. The product was obtained after freeze-drying, named Fe/MMT-Na. When no MMT-Na was added, the resulting product was named Schwertmannite (Sch).

Synthesis of ferrihydrite

To synthesis ferrihydrite, 50 mL of deionized water was mixed with 4.0 g $Fe(NO_3)_3{\cdot}9H_2O$, and 33 mL of 1 M NaOH was added while vigorously stirring. Then the solution was

centrifuged, and the solid was washed several times with deionized water. Ferrihydrite was obtained after freeze-drying.

Synthesis of lepidocrocite

Typically, 2.7 g $FeCl_3 \cdot 6H_2O$ was added to 100 mL of deionized water, and the solution was heated to 70 ℃ for 24 h. Then the solution was centrifuged, and the yellow solid was washed several times with deionized water. The resulting product was named lepidocrocite.

Synthesis of magnetite

Typically, 2.5 mmol $FeCl_2 \cdot 4H_2O$ and 75.0 mmol NH_4Cl were added to 15 mL of water. Then 5 mL of $NH_3 \cdot H_2O$ was dropwise added under vigorous stirring. After 5 min, the solution was transferred into a Teflon-lined stainless-steel autoclave, maintained at 140 °C for 16 h. Then the resultant samples were washed three times. The product was obtained after freeze-drying, named magnetite.

Enzyme-like catalytic activity of samples

The peroxidase (POD)-like activity of samples was tested using TMB as the substrate. The absorbance of the colorimetric reaction product was measured at a certain reaction time via a microplate reader. In a typical test, MMT-Na or Fe/MMT-Na (final concentration 67 μg/mL) was added to 100 μL saline. Then 100 μL H_2O_2 and 100 μL TMB were added. The final concentration of H_2O_2 and TMB was 40 mM and 0.4 mM, respectively. In addition, the POD-like activity of other products was also tested. The kinetic parameters were calculated by the plot linear-fitting based on the Lineweaver-Burk double reciprocal equation that comes from the Michaelis-Menten equation:[1]

$$\frac{1}{v} = \frac{K_m}{V_{max}[S]} + \frac{1}{V_{max}} \quad (1)$$

where [*S*] denotes the concentration of substrate, V_{max} represents the maximal reaction velocity, *v* represents the initial velocity, and K_m denotes the Michaelis constant. The test for oxidase (OXD)-like activity of the samples was similar to the procedure described above for POD-like activity, with the exception that H_2O_2 was not added.

Colorimetric detection of H_2O_2

In 100 μL saline, Fe/MMT-Na (67 μg/mL) was added. Then, various concentrations of H_2O_2 (100 μL) were sequentially added. Finally, TMB solution (100 μL, final concentration 0.4 mM) was added for incubation for 5 minutes. After that, the absorbance values were recorded by a microplate reader.

Selectivity of colorimetric sensor

In 100 μL saline, Fe/MMT-Na (67 μg/mL) was added. Then, a variety of ions or small biological molecules were sequentially added (final concentration 50 mM). The concentration of the interfering substances was 10 times higher than the concentration of H_2O_2. Finally, TMB solution (100 μL, final concentration 0.4 mM) was added for incubation for 5 minutes. After that, the absorbance values were recorded by a microplate reader.

Supplementary Results

Effects of molten salt on Fe atoms in MMT

The iron valence state of MMT-Na was inspected via X-ray photoelectron spectroscopy (XPS) (Fig. S1a, ESI†). For the 2p spectrum, the consistent $2p_{3/2}$ peak position at 711.0 eV corresponds to Fe (III) in MMT-Na.[2] The iron content in MMT before and after molten salt treatment was 2.59% and 2.91%, respectively, measured by an inductively coupled plasma

optical emission spectrometer (ICP-OES). An X-ray absorption fine structure (XAFS) was used to investigate the valence state and local structure of the Fe atom. Fig. S1b shows that the near-edge adsorption energy of Fe K-edge in MMT and MMT-Na almost coincides with the reference sample Fe_2O_3, indicating the valence state of Fe in the two samples is +3. It can be seen from the *k*-space fitting results of MMT and MMT-Na (Fig. S1c, ESI†), that the fitting curves of the two samples nearly overlap, demonstrating that the local structure of the Fe atom in the two samples remains the same.[3] Fourier transformations of Fe K-edge EXAFS in R-space for MMT and MMT-Na are shown in Fig. S1d, ESI†. The first peak at 1.6 Å is assigned to oxygen atoms surrounding octahedral Fe, and another peak at 2.6 Å is preponderantly due to Fe-Si and Fe-Al single-scattering contributions.[4]

Calculation method of B/L

IR spectroscopy of the adsorption of pyridine (Py-FTIR) tests was carried out to investigate the nature of the acid sites on the surface of catalysts. The band at 1446 cm^{-1} was assigned to the Lewis acid (L) sites coordinated by pyridine. The band at 1545 cm^{-1} was related to the pyridine in Brønsted acid (B) site. The quantification of B and L acid site ratio (B/L) was done from the characteristic peak area of 1545 cm^{-1} for B and 1446 cm^{-1} for L. For MMT-Na, the concentration of B and L acid site was 21.29 and 43.45 μmol/g, respectively. The B/L value was calculated to be 0.49. For Fe/MMT-Na, the concentration of B and L acid sites was 171.34 and 369.15 μmol/g, respectively. The B/L value was calculated to be 0.46.

Enzyme-like catalytic activity of MMT-Na

In Fig. S3, ESI†, under the same conditions, MMT-Na shows the highest absorbance at 652 nm, indicating that MMT-Na exhibits the highest POD-like activity. The POD-like relative

catalytic activity of MMT-Na is 14.6 times higher than that of MMT. We also investigated the effect of molten salts on the POD-like activity of products. The experimental results showed that the MMT-Na has the highest POD-like activity (Fig. S4, ESI†). This is due to the MMT can only be exfoliated adequately in $NaNO_3$ molten salt, thus exposing more reactive sites. Furthermore, we found that both MMT and MMT-Na have negligible oxidase (OXD)-like activity (Fig. S5, ESI†).

Identify the active site of MMT-Na

XRD patterns showed that there was no chemical reaction between Fe_2O_3 and SiO_2 in $NaNO_3$ molten salt, and the mixture of Fe_2O_3 and SiO_2 had negligible POD-like activity (Fig. S6, ESI†). This indicates that there is no chemical reaction between iron oxides and SiO_2 in $NaNO_3$ molten salt. As a comparison, the POD-like activity of four kinds of iron-bearing minerals (i.e., ferrihydrite, lepidocrocite, magnetite, and hematite) was assessed, and it was found that all of them show extremely low POD-like activity (Fig. S7, ESI†), thus excluding the influence of other iron-bearing minerals in MMT on the colorimetric reaction. To confirm whether structural iron is the active site, we replaced MMT with Hectorite, which has a similar structure to MMT but does not contain structural iron. The chemical compositions of MMT and Hectorite are listed in Table S1, ESI†. As shown in Fig. S8a, ESI†, the prepared product Hectorite-Na reveals extremely low POD-like activity, indicating that structural iron is indeed the active site. Furthermore, when structural iron is shielded by 2,2'-bipyridine (BPY), the POD-like activity of the MMT-Na disappears, which provides further evidence (Fig. S8b, ESI†). Since transition metal ions can act as Lewis acid sites, we hypothesize that the structural iron in MMT-Na acts as the Lewis acid sites. To prove that, PO_4^{3-} Lewis base

was used to screen the Lewis acid sites on MMT-Na. In Fig. S9, ESI†, when PO_4^{3-} was added to the reaction system, the POD-like activity of the MMT-Na disappeared, which validated our conjecture. The above results prove that structural iron in MMT-Na is the main active site, and the contact between the active sites and the substrate TMB is sufficient after exfoliation, resulting in a significant improvement in the POD-like activity of MMT-Na.

Identify the active site of Fe/MMT-Na

We notice that when iron sulfate hydrate is used as an iron source, and no MMT is added, it will hydrolyze and form Schwertmannite (Sch) (Fig. S10, ESI†). Due to its excellent cation exchangeability, MMT-Na could prevent the hydrolysis of iron sulfate hydrate when MMT-Na was added to the reaction system. Eventually, Fe species were fixed within the interlayer space of MMT-Na (Fig. S11, ESI†). Two other experimental results also confirmed the correctness of this statement. The XPS characterization demonstrated that Fe/MMT-Na contained no sulfur element (Fig. S12, ESI†); when iron nitrate nonahydrate replaced iron sulfate hydrate as an iron source, there was no obvious difference in the peroxidase (POD)-like activity of the products (Fig. S13, ESI†). Moreover, subsequent experimental results indicated that the chloride ions in the solvent (Fig. S14, ESI†) and the leached metal ions (Fig. S15, ESI †) did not promote the colorimetric reaction. Such a substantial enhancement of POD-like activity can be ascribed to the iron ions within the interlayers rather than leaked iron ions or Cl^- in the solution.

Supplementary reaction mechanism analysis

Temperature programmed reduction of hydrogen (H_2-TPR) profiles of MMT-Na and Fe/MMT-Na in Fig. S18 reveals that the peak at 352 °C for Fe/MMT-Na can be ascribed to

the reduction of Fe^{3+} to Fe^{2+} and the reduction of structural iron within MMT at temperatures between 750 °C and 900 °C.[5] O-Phenylenediamine (OPD), 2,2'-azinobis(3-ethylbenzothiazoline-6-sulfonic acid ammonium salt) (ABTS), and TMB are usually used as the substrates for colorimetric reactions. Their common structural feature is that they contain nitrogen atoms, which can act as electron donors. In Fig. S20, ESI†, only Fe/MMT-Na shows good catalytic oxidation to the three substrates, and the relative catalytic activities follow the order of Fe/MMT-Na > MMT-Na > MMT.

Stability and reproducibility of colorimetric sensor

After four months of storage, the absorbance value of the colorimetric sensor fabricated by Fe/MMT-Na did not decrease, suggesting good stability of the Fe/MMT-Na (Fig. S22, ESI†). In addition, the reproducibility of the Fe/MMT-Na colorimetric sensor for the detection of H_2O_2 is also satisfactory (Fig. S23, ESI†).

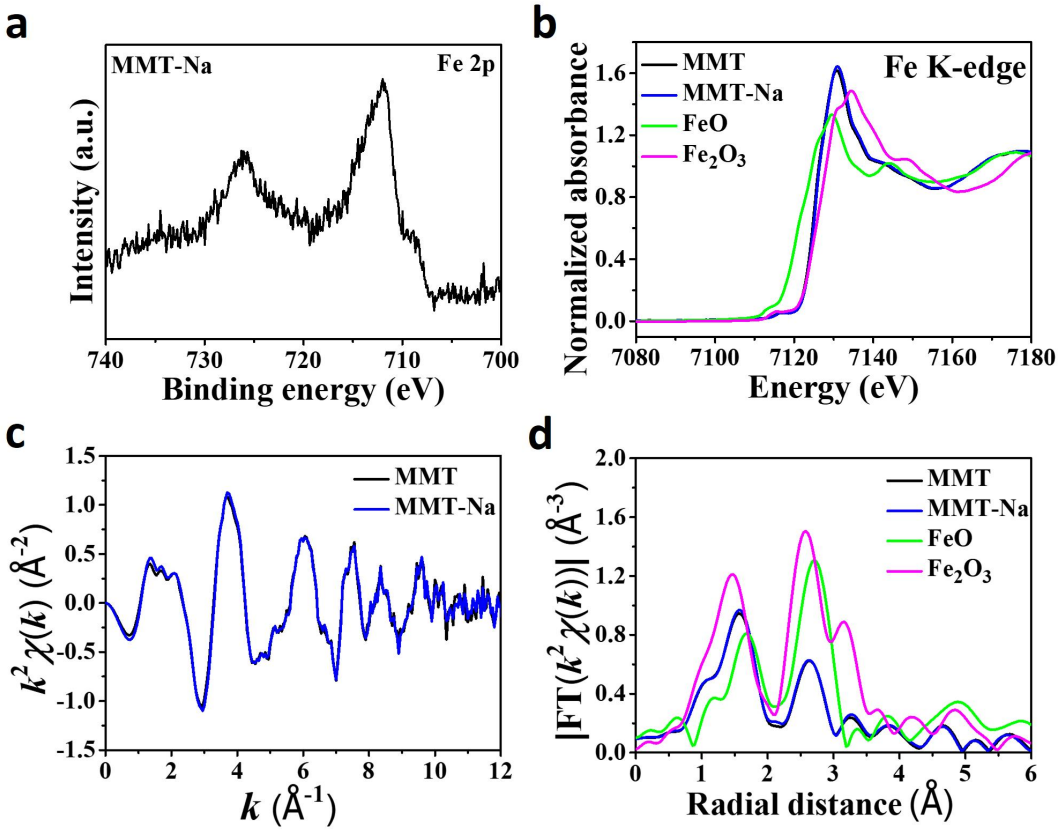

Fig. S1. (a) High-resolution XPS spectra of Fe for MMT-Na. (b) Fe K-edge XANES spectra, (c) FT-EXAFS curves at *k* space, and (d) Fourier transformations of Fe K-edge EXAFS in R-space for MMT and MMT-Na.

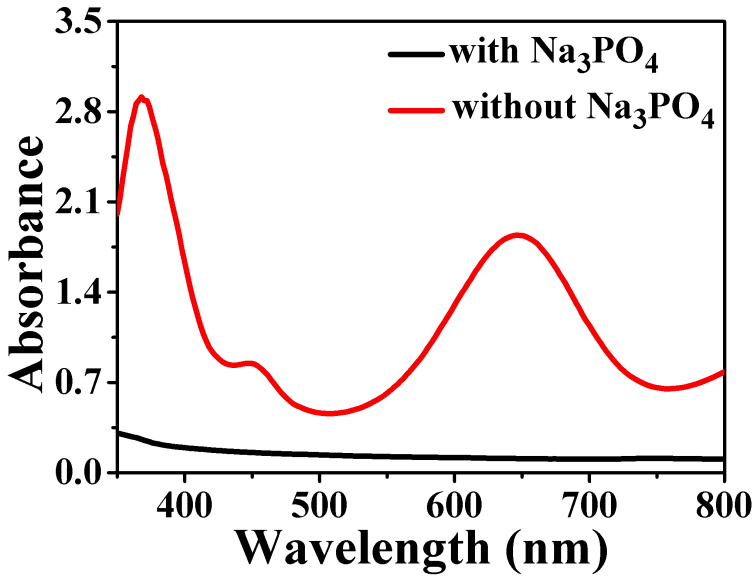

Fig. S2. The absorbance of Fe/MMT-Na in a POD-like reaction with Na_3PO_4 and without Na_3PO_4.

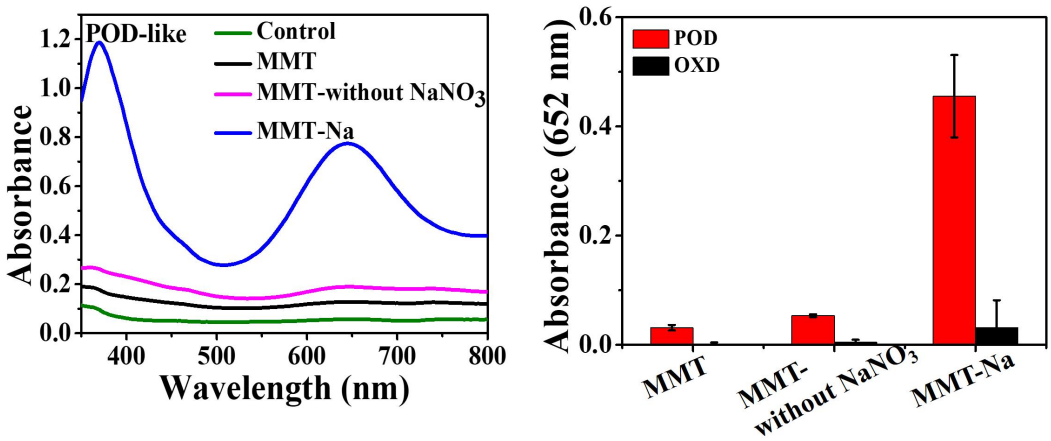

Fig. S3. Absorption curves of different samples in POD-like reaction and the absorbance value of samples in POD-like and OXD-like reactions.

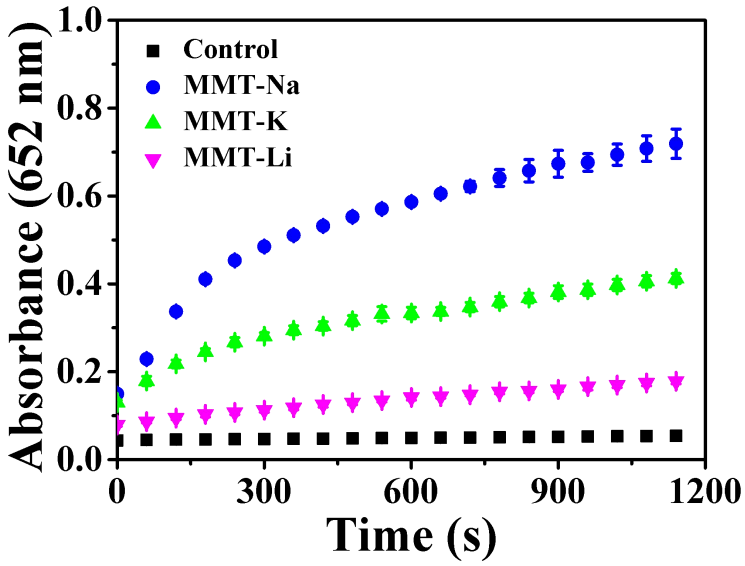

Fig. S4. Time-dependent absorbance of TMB colorimetric reaction catalyzed by MMT-Na, MMT-K, and MMT-Li in POD-like reaction. The concentrations of samples, TMB, and H_2O_2 were 67 μg/mL, 0.4 mM, and 40 mM, respectively.

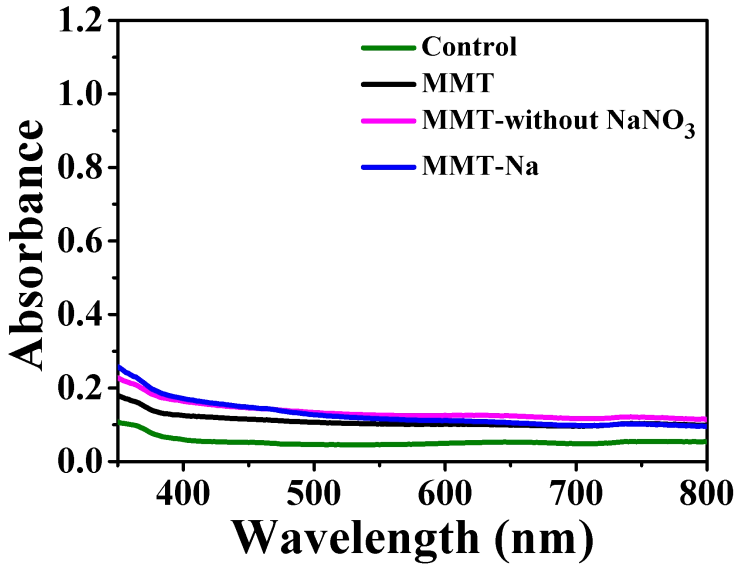

Fig. S5. Absorbance of MMT, MMT-without $NaNO_3$, and MMT-Na in OXD-like reaction. The concentrations of samples and TMB were 67 μg/mL and 0.4 mM, respectively.

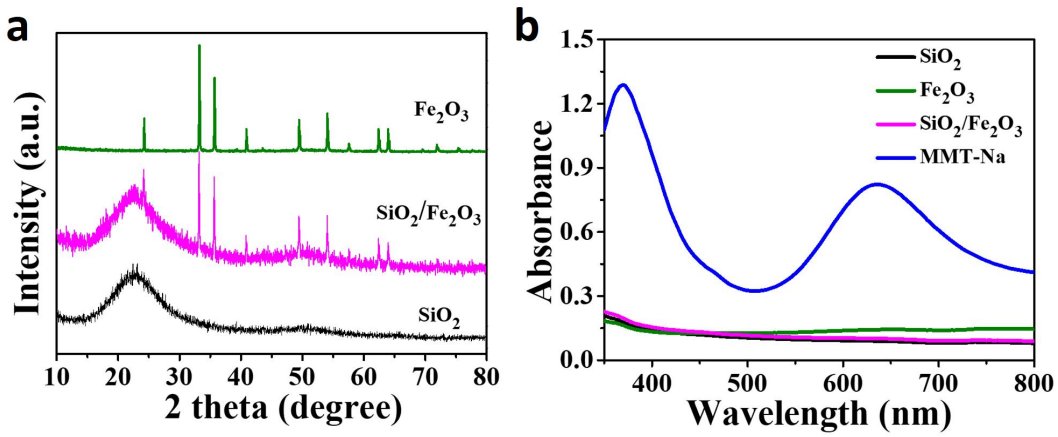

Fig. S6. (a) XRD patterns of Fe_2O_3, SiO_2, and SiO_2/Fe_2O_3. (b) The absorbance of different samples in a POD-like reaction. The concentrations of samples, TMB, and H_2O_2, were 67 μg/mL, 0.4 mM, and 40 mM, respectively.

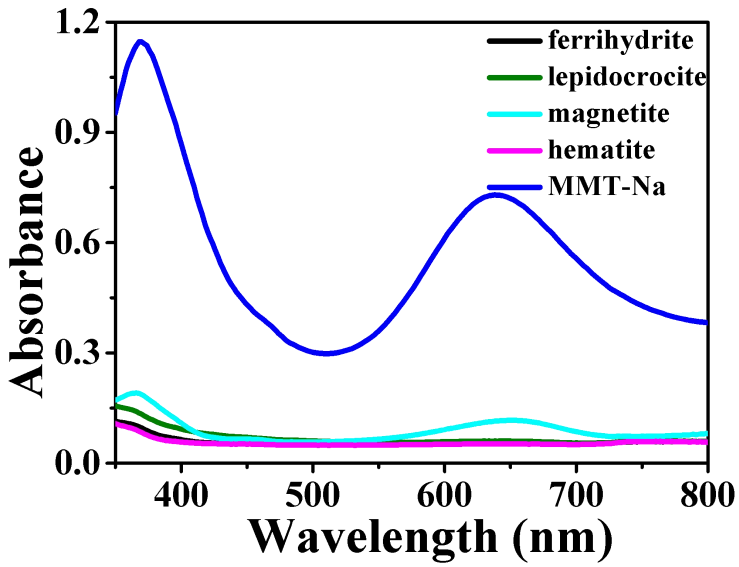

Fig. S7. The absorbance of ferrihydrite, lepidocrocite, magnetite, hematite, and MMT-Na in a POD-like reaction. The concentrations of samples, TMB, and H_2O_2 were 67 μg/mL, 0.4 mM, and 40 mM, respectively.

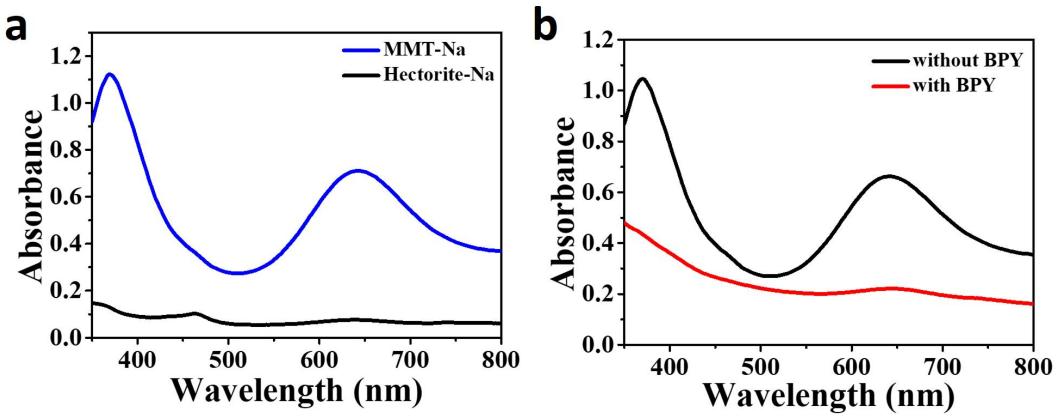

Fig. S8. (a) The absorbance of Hectorite-Na and MMT-Na in a POD-like reaction. The concentration of samples, TMB, and H_2O_2 were 67 μg/mL, 0.4 mM, and 40 mM, respectively. (b) The absorbance of MMT-Na in a POD-like reaction with BPY and without BPY. The concentration of BPY was 0.5 mM.

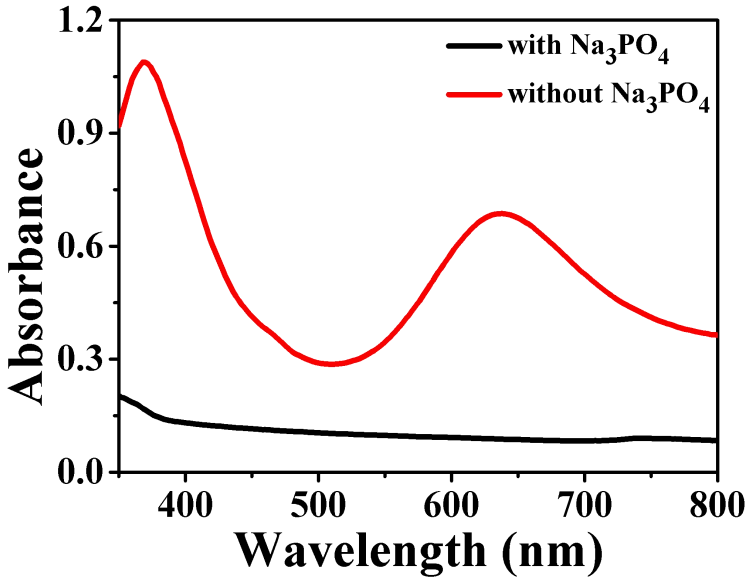

Fig. S9. The absorbance of MMT-Na in a POD-like reaction with Na_3PO_4 and without Na_3PO_4. The concentrations of the samples, TMB, H_2O_2, and Na_3PO_4 were 67 μg/mL, 0.4 mM, 40 mM, and 20 mM, respectively.

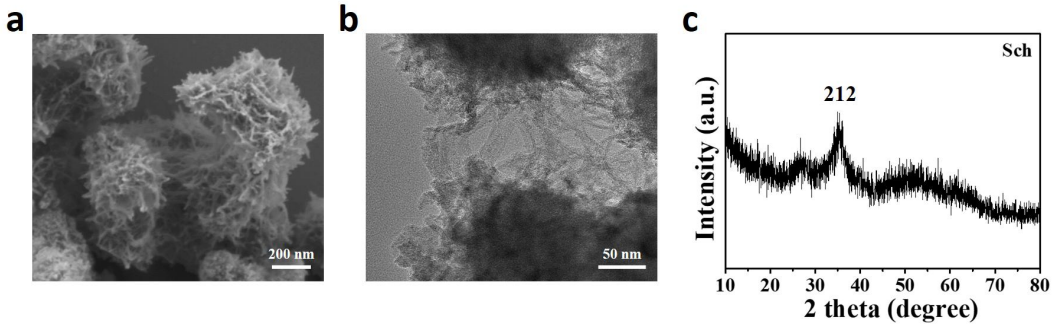

Fig. S10. (a) SEM, (b)TEM, and (c)XRD pattern of Schwertmannite (Sch).

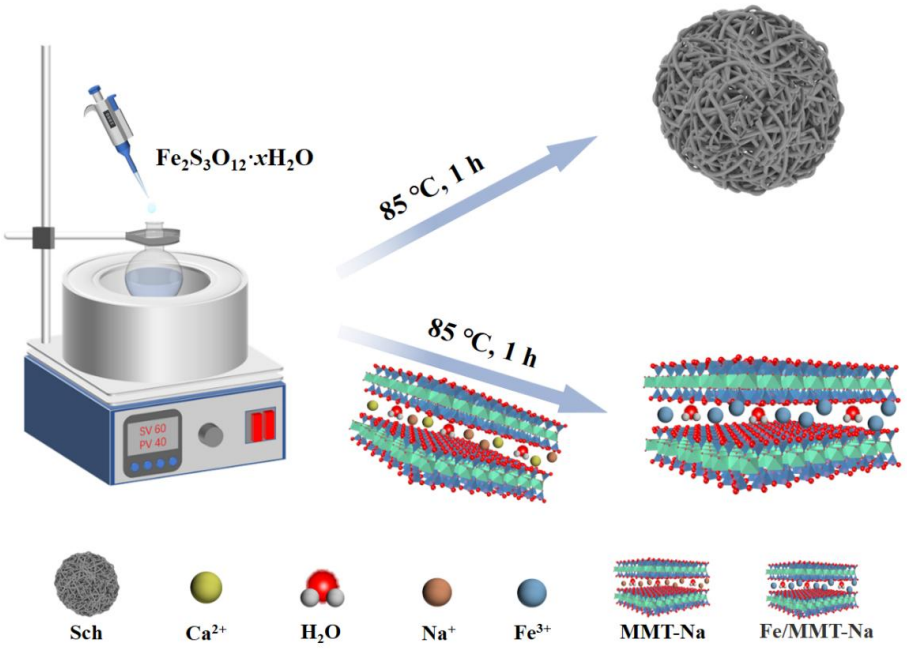

Fig. S11. Schematic diagram of the synthesis of Fe/MMT-Na and Schwertmannite (Sch).

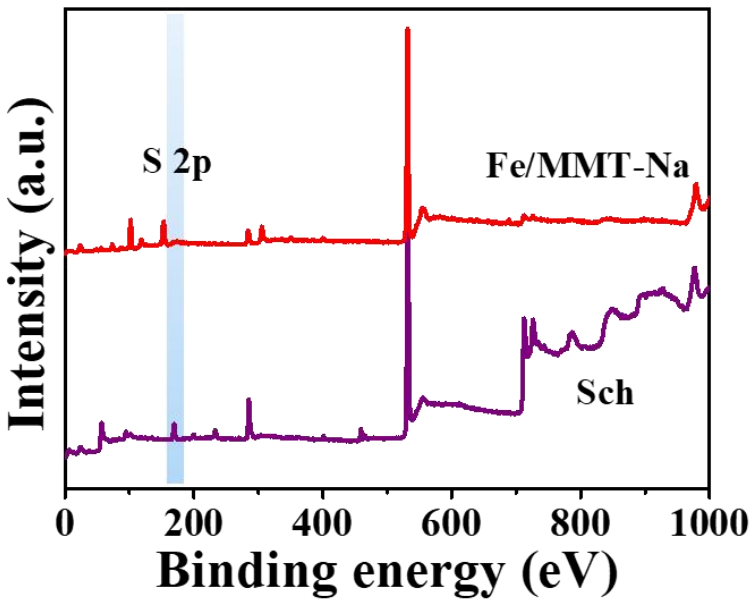

Fig. S12. XPS survey spectrum of Fe/MMT-Na and Schwertmannite (Sch).

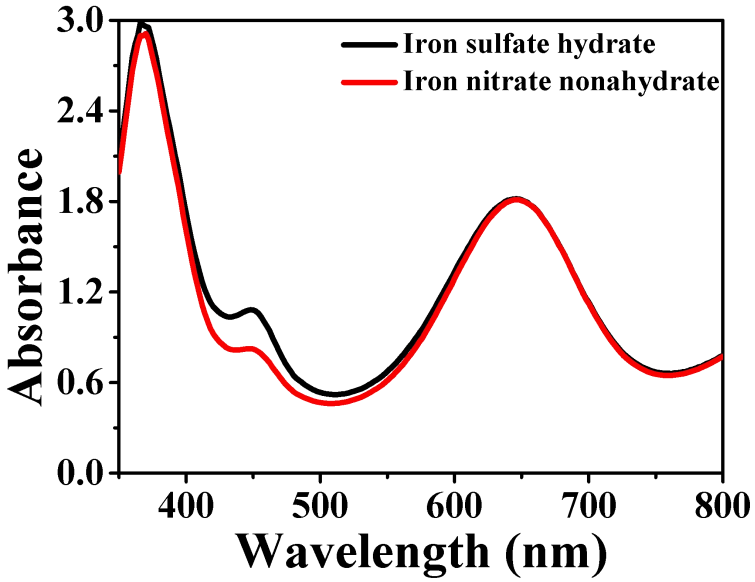

Fig. S13. The absorbance of prepared products from different iron sources in a POD-like reaction.

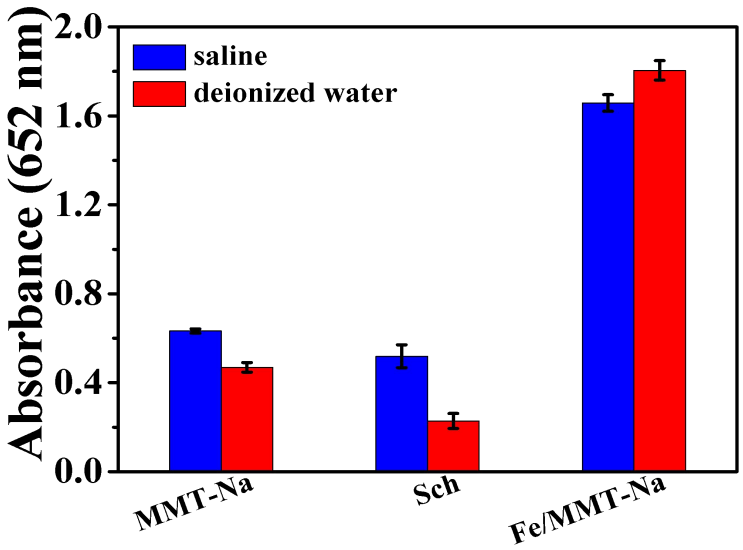

Fig. S14. Absorbance of TMB oxidation catalyzed by different products in saline and deionized water.

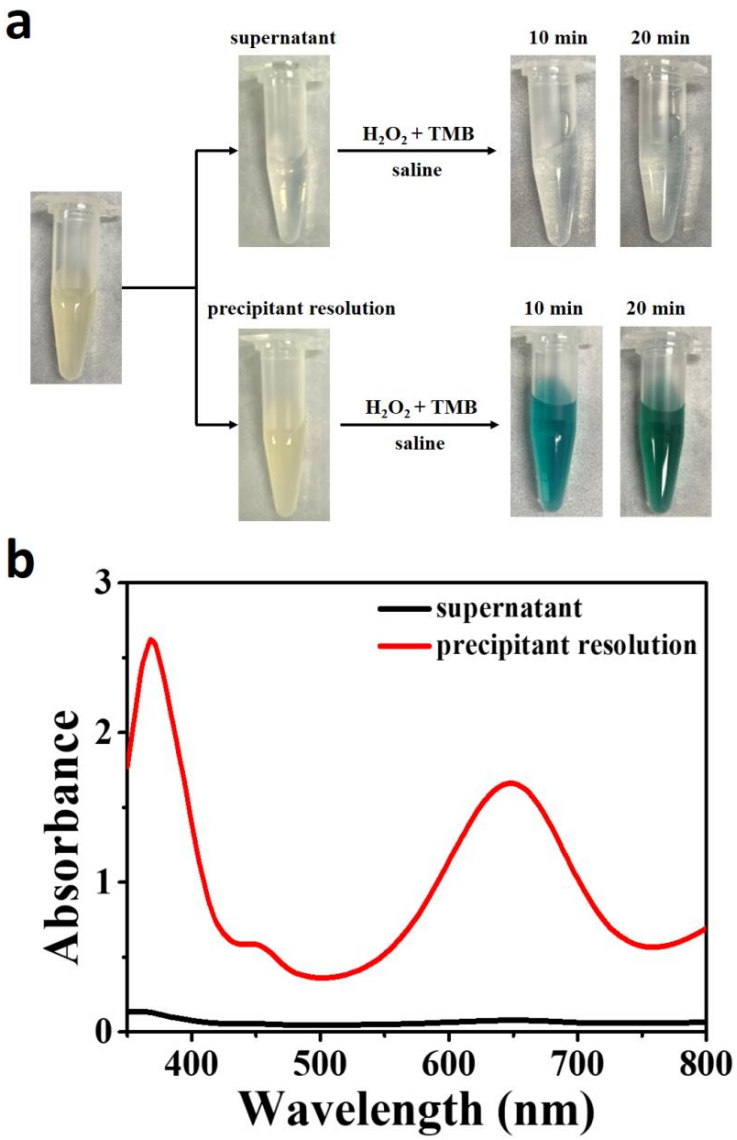

Fig. S15. (a) Photographs and (b) absorption curves of Fe/MMT-Na supernatant and precipitant resolution at various reaction times.

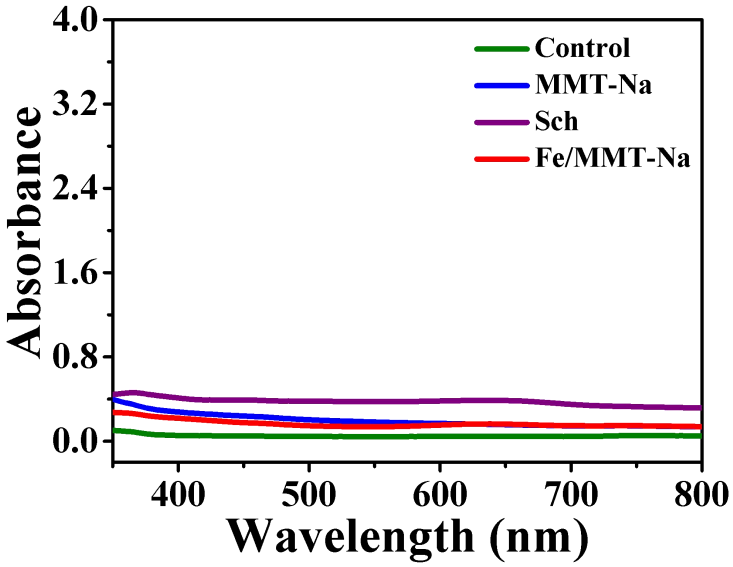

Fig. S16. The absorbance of MMT-Na, Sch, and Fe/MMT-Na in an OXD-like reaction. The concentrations of samples and TMB were 67 μg/mL and 0.4 mM, respectively.

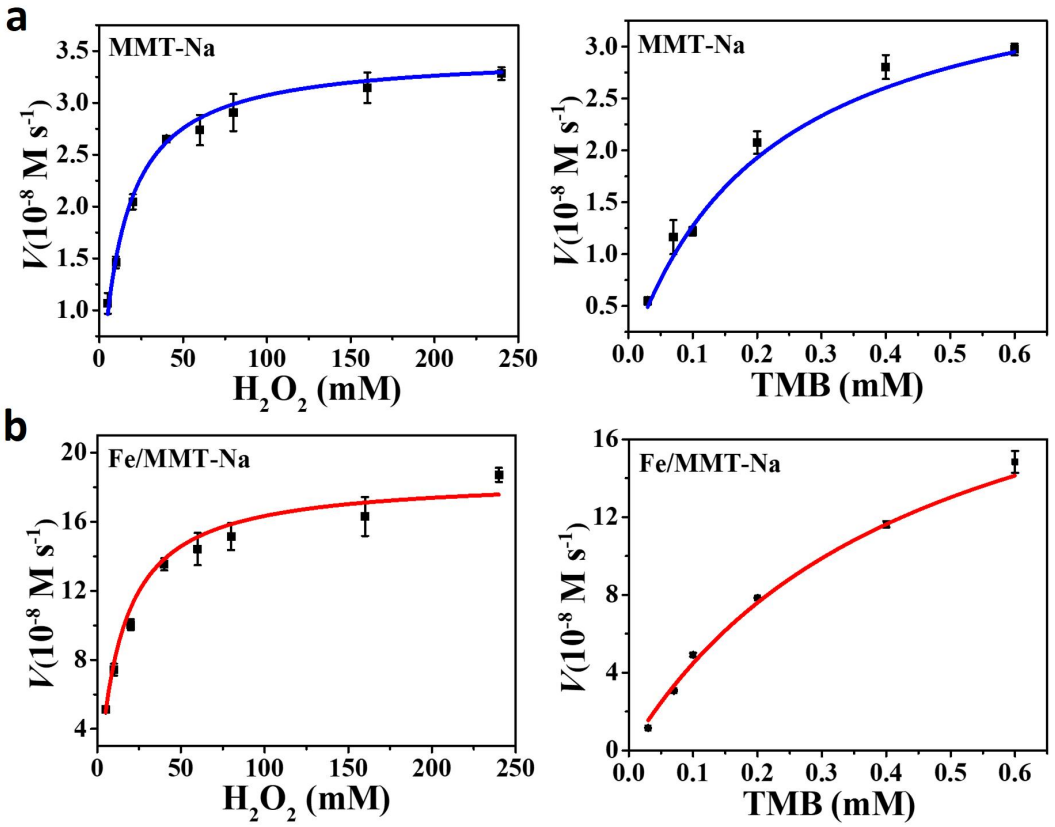

Fig. S17. Steady-state kinetic analyses for (a) MMT and (b) Fe/MMT-Na using the Michaelis-Menten equation as the non-linear least-squares regression.

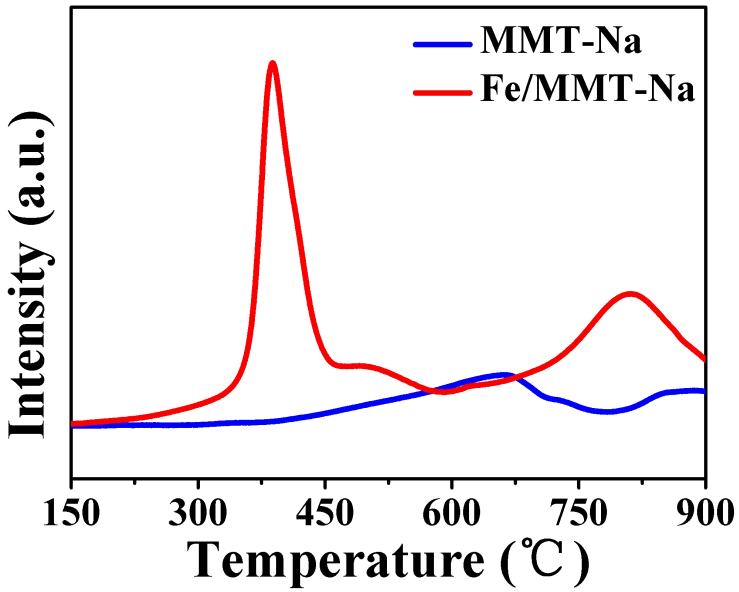

Fig. S18. H_2-TPR of MMT-Na and Fe/MMT-Na.

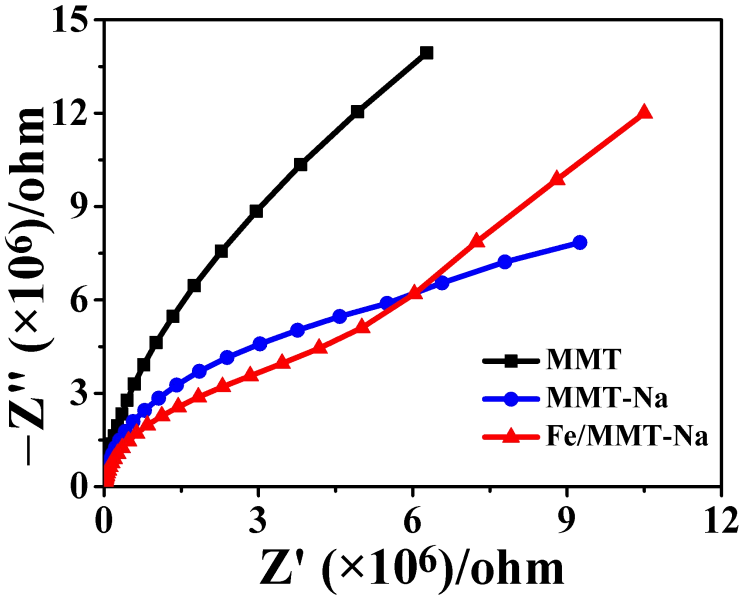

Fig. S19. EIS of MMT, MMT-Na, and Fe/MMT-Na.

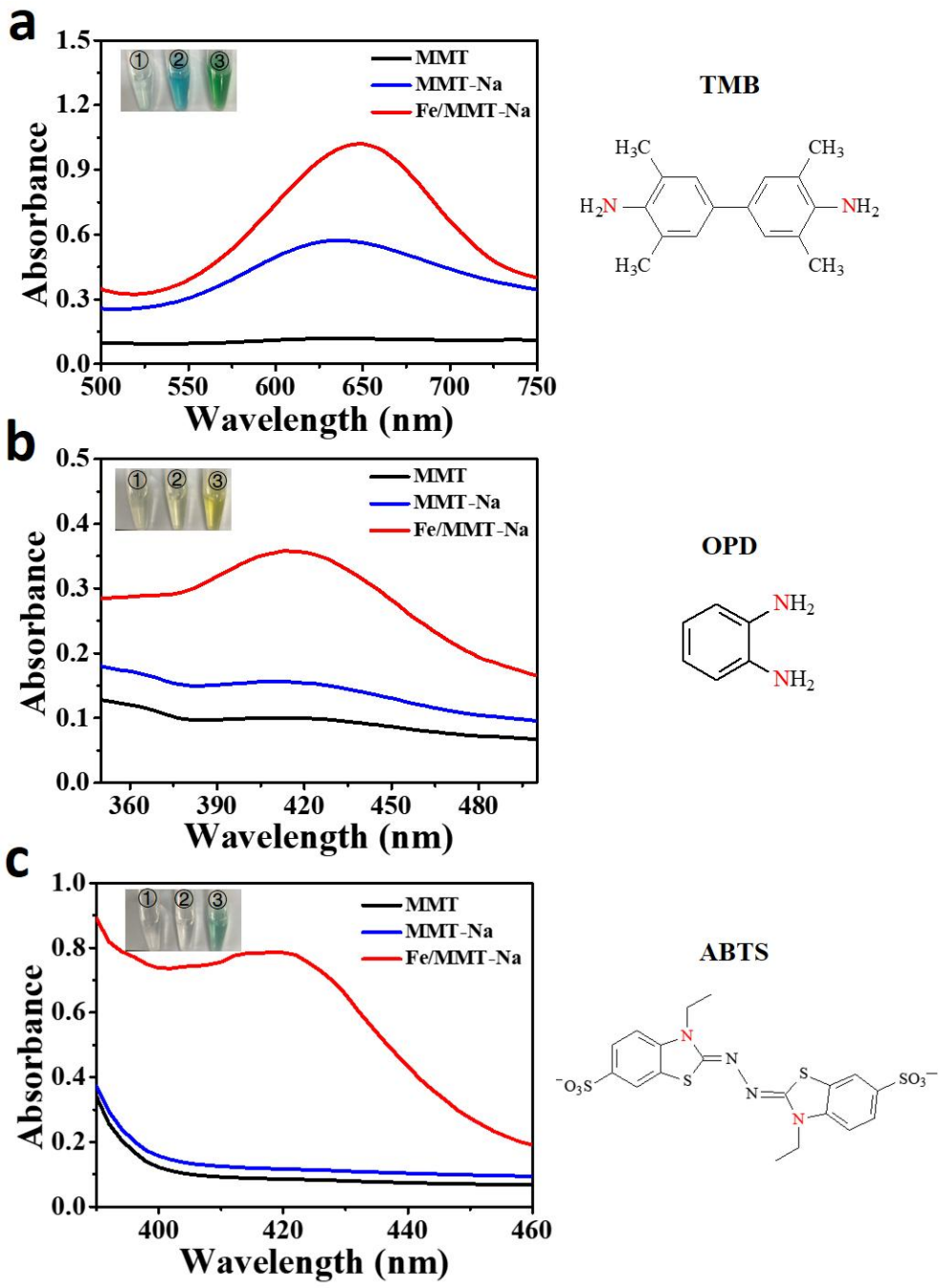

Fig. S20. The absorption spectra of (a) TMB, (b) OPD, and (c) ABTS substrates were catalyzed by different nanozymes and the chemical structure of the substrates. Inset: corresponding photographs of the reaction system.

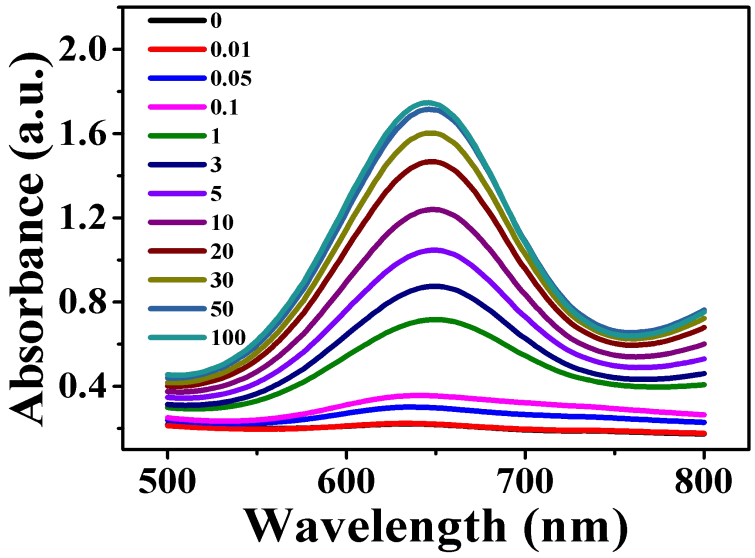

Fig. S21. UV-vis absorption spectra of the proposed colorimetric biosensor with different H_2O_2 concentrations (unit: mM).

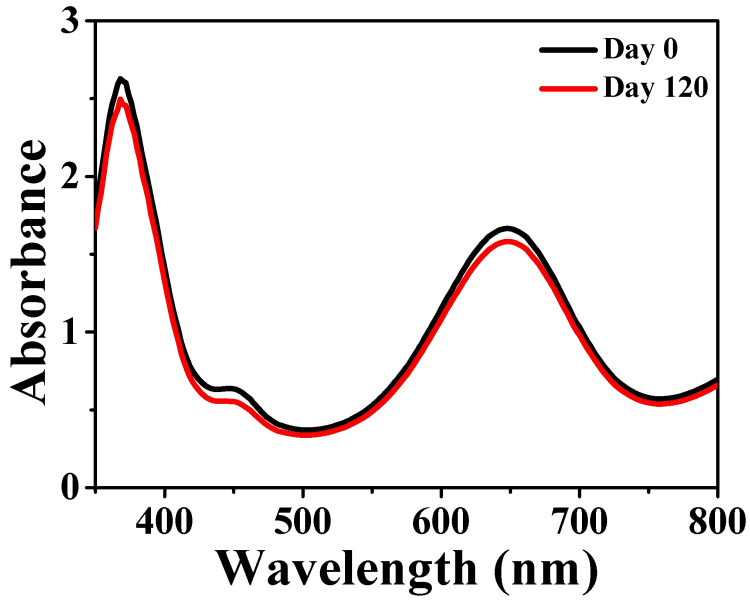

Fig. S22. Stability of the Fe/MMT-Na colorimetric sensor for the detection of H_2O_2.

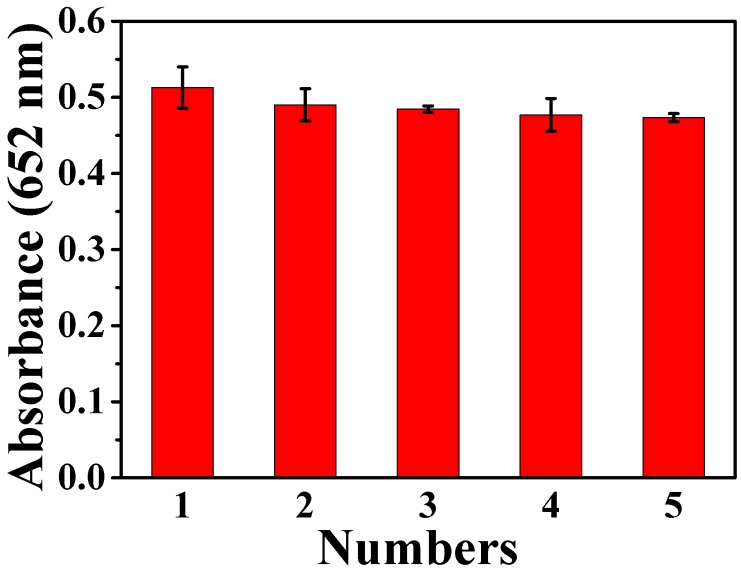

Fig. S23. Reproducibility of the Fe/MMT-Na colorimetric sensor for the detection of H_2O_2.

Table S1 XRF analysis of MMT and Hectorite.

Samples	SiO_2	Al_2O_3	Fe_2O_3	CaO	MgO	others
MMT	68.38	16.36	5.67	4.53	3.70	1.36
Hectorite	70.34	0.25	-	0.27	24.29	4.85

Table S2 Comparison of the kinetic parameters of different nanozymes.

Samples	[*E*] (M)	Substance	K_m (mM)	V_{max} (M s^{-1})	K_{cat} (s^{-1})	Ref.
MMT-Na	2.6×10^{-8}	TMB	0.21	4.05×10^{-8}	1.56	This
	2.6×10^{-8}	H_2O_2	12.93	3.47×10^{-8}	1.33	work
Fe/ MMT-Na	5.4×10^{-8}	TMB	1.18	53.62×10^{-8}	9.93	This
	5.4×10^{-8}	H_2O_2	18.76	13.85×10^{-8}	2.56	work
Fe-MOF	4.9×10^{-5}	TMB	2.6	5.6×10^{-8}	0.0011	6
	4.9×10^{-5}	H_2O_2	1.3	2.5×10^{-8}	0.0005	
Pt hollow	7×10^{-6}	TMB	0.81	1.2×10^{-7}	0.014	7
nanodendrites	7×10^{-6}	H_2O_2	6.9	9.9×10^{-8}	0.0069	
Cu-N-C	2.68×10^{-6}	TMB	3.76	75.05×10^{-8}	0.075	8
	2.68×10^{-6}	H_2O_2	19.94	20.07×10^{-8}	0.283	

[*S*] represents the concentration of Fe in MMT-Na and Fe/ MMT-Na, which was obtained by ICP-OES; V_{max}: maximum reaction velocity; K_m: Michaelis constant; K_{cat} is the catalytic constant that equals V_{max}/[*E*]; MOF: Metal-Organic Framework.

Table S3 Comparison of analytical parameters for the detection of H_2O_2 by different colorimetric sensors.

Nanozymes	pH value	Linear range (mM)	Detection limit (μM)	Ref.
Ru/PC	6.0	0.005-1.5	3.8	[9]
Fe-N-C SAzymes	3.0	0.5-100.0	-	[10]
SiO_2@TiO_2/PDI-OH	4.0	0.0002-0.04	0.076	[11]
Ag@TPE-SiO_2 NPs	7.4	0.005-0.16	2.1	[12]
BSA-RuO_2NPs	6.0	0.002-0.8	1.8	[13]
$Co_{0.5}Ni_{0.5}Fe_2O_4$-MMT	4.0	0.0005-0.02	0.565	[14]
$NiCo_2S_4$ NPs	4.0	0.01-0.7	8.0	[15]
Fe/MMT-Na	7.0	0.05-100.0	10.0	This work

Ru/PC: ruthenium/porous carbon; SAzymes: single-atom nanozymes; PDI-OH: perylenediimide; TPE: tetraphenylethene; BSA: bovine serum albumin; MMT: montmorillonite; NPs: nanoparticles; Fe/MMT-Na: Fe^{3+} exchange exfoliated montmorillonite.

References

1 B. Jiang, D. Duan, L. Gao, M. Zhou, K. Fan, Y. Tang, J. Xi, Y. Bi, Z. Tong, G. F. Gao, N. Xie, A. Tang, G. Nie, M. Liang and X. Yan, *Nat. Protoc.*, 2018, **13**, 1506-1520.

2 G. X. Huang, C. Y. Wang, C. W. Yang, P. C. Guo and H. Q. Yu, *Environ. Sci. Technol.*, 2017, **51**, 12611-12618.

3 D. Soltermann, M. Marques Fernandes, B. Baeyens, R. Dahn, P. A. Joshi, A. C. Scheinost and C. A. Gorski, *Environ. Sci. Technol.*, 2014, **48**, 8688-8697.

4 D. Vantelon, E. Montarges-Pelletier, L. J. Michot, M. Pelletier, F. Thomas and V. Briois, *Phys. Chem. Miner.*, 2003, **30**, 44-53.

5 X. Liang, F. Qi, P. Liu, G. Wei, X. Su, L. Ma, H. He, X. Lin, Y. Xi, J. Zhu and R. Zhu, *Appl. Clay. Sci.*, 2016, **132-133**, 96-104.

6 W. Xu, L. Jiao, H. Yan, Y. Wu, L. Chen, W. Gu, D. Du, Y. Lin and C. Zhu, *ACS Appl. Mater. Interfaces*, 2019, **11**, 22096-22101.

7 C. Ge, R. Wu, Y. Chong, G. Fang, X. Jiang, Y. Pan, C. Chen and J. J. Yin, *Adv. Funct. Mater.*, 2018, **28**, 1801484.

8 Y. Wu, J. Wu, L. Jiao, W. Xu, H. Wang, X. Wei, W. Gu, G. Ren, N. Zhang, Q. Zhang, L. Huang, L. Gu and C. Zhu, *Anal. Chem.*, 2020, **92**, 3373-3379.

9 S. Feng, M. Ming, M. Wang, X. Wang, D. He, P. Jiang and Y. Chen, *Chem. Commun.*, 2020, **56**, 12347-12350.

10 L. Jiao, W. Xu, H. Yan, Y. Wu, C. Liu, D. Du, Y. Lin and C. Zhu, *Anal. Chem.*, 2019, **91**, 11994-11999.

11 Q. Liu, S. Cao, Q. Sun, C. Xing, W. Gao, X. Lu, X. Li, G. Yang, S. Yu and Y. Chen, *J. Hazard. Mater.*, 2022, **436**, 129321.

12 X. Huang, H. Zhou, Y. Huang, H. Jiang, N. Yang, S. A. Shahzad, L. Meng and C. Yu, *Biosens. Bioelectron.*, 2018, **121**, 236-242.

13 S. B. He, P. Balasubramanian, Z. W. Chen, Q. Zhang, Q. Q. Zhuang, H. P. Peng, H. H. Deng, X. H. Xia and W. Chen, *ACS Appl. Mater. Interfaces*, 2020, **12**, 14876-14883.

14 X. Zhu, H. Li, T. Wu, H. Zhao, K. Wu, W. Xu, F. Qin, W. Chen, J. Zheng and Q. Liu, *Nano Res.*, 2022, DOI: 10.1007/s12274-022-4594-x.

15 M. Lian, M. Liu, X. Zhang, W. Zhang, J. Zhao, X. Zhou and D. Chen, *ACS Appl. Mater. Interfaces*, 2021, **13**, 53599-53609.